Ceramics International 46 (2020) 10023–10028

Contents lists available at ScienceDirect

Ceramics International

journal homepage: www.elsevier.com/locate/ceramint

Understanding the growth of NiSe nanoparticles on reduced graphene oxide as efficient electrocatalysts for methanol oxidation reaction

Jingchun Jia[a,b,*], Linghui Zhao[a,b], Ying Chang[a,c], Meilin Jia[a,**], Zhenhai Wen[b]

[a] College of Chemistry and Environmental Science, Inner Mongolia Key Laboratory of Green Catalysis and Inner Mongolia Collaborative Innovation Center for Water Environment Safety, Inner Mongolia Normal University, Hohhot, 010022, China

[b] CAS Key Laboratory of Design and Assembly of Functional Nanostructures, and Fujian Provincial Key Laboratory of Nanomaterials, Fujian Institute of Research on the Structure of Matter, Chinese Academy of Sciences, Fuzhou, Fujian, 350002, PR China

[c] Fujian Provincial Key Laboratory of Fire Retardant Materials, College of Materials, Xiamen University, Xiamen, 361005, China

ARTICLE INFO

Keywords:
Methanol oxidation reaction
Selenylation
NiSe
Nanoparticles

ABSTRACT

With the development of direct methanol fuel cell (DMFC), methanol oxidation reaction (MOR) becomes the crux of the application of DMFC, and the preparation of cheap, efficient MOR electrocatalyst is still the focus of researchers. Hence, we have prepared NiSe/RGO nanoparticles by a simple and universal way using pyrolyzation and selenylation. The MOR of NiSe/RGO is tested in 0.5 M MeOH/1 M KOH solution. Compared with the precursor Ni, NiSe/RGO-550 has outstanding performance for MOR with onset potential is 1.35 V *vs.* RHE, and 59.84 mA cm^{-2} for peak current density, and it can stable catalytic oxidation of methanol more than 4000 s. Because of the augment of active sites after selenization and the load of RGO enhanced electroconductibility, NiSe/RGO-550 has remarkable performance for MOR. This work provides the possibility of high performance, low cost catalysts for energy storage, conversion and practical applications.

1. Introduction

With the shortage of non-renewable energy and the worsening of environmental pollution, the search for new green energy attracts global attention [1–3]. Among the new green energy sources, methanol direct fuel cell has become a candidate of new energy because of its preponderances of supernal volume energy density, supernal energy conversion efficiency and low toxic of the discharge [1,2,4–7]. The Pt-based materials have excellent methanol oxidation properties at the anode of direct methanol fuel cell (DMFC) [8–16], but it is difficult to large-scale application that high price and precious metal [17]. Therefore, it is indispensable to search for non-precious metals anode catalysts with excellent methanol oxidation performance with low price.

In recent years, nickel based materials have been diffusely used in energy conversion and storage reactions due to their surface oxidation properties, such as oxygen evolution reaction (OER) [18–22], hydrogen evolution reaction (HER) [23,24], and methanol oxidation reaction (MOR) [25,26]. Furthermore, there are much more researches on different nickel-based materials as catalysts for MOR. Massive nickel dispersed on graphene by electro-deposition better than the metal Ni for oxidize methanol [27]. PdNi nanoparticles catalyst was prepared by metal ion chemical reduction which has better MOR performance than Ni [28]. Ni_2Co_2 was prepared by electrodeposition has higher oxidation current density about 58 mA cm^{-2} higher than pristine Ni, and the best durability for 1200 s [29]. Mn–$Ni(OH)_2$ with hierarchical hollow structure was prepared by sacrificial templating method with good durability and stability [1]. $NiCo_2O_4$-rGO hybrid was prepared by two-step solution phase method with low potential and outstanding catalytic durability that current density kept 95% after 3600s [30]. 3D mesoporous $NiCo_2O_4$ nanosheet was with onset potential (0.19 V) and the current density remained 95% based on the initial value after 1000 s stability test [31]. Numerous experimental studies show that nickel-based material oxides, alloys and modified nickel-based materials have more catalytic activity sites and a better oxidation methanol performance. (The MOR properties of nickel-based materials are compared in Table S1)

Due to the excellent MOR properties of nickel-based materials, we designed and prepared Ni precursor by pyrolysis method, and obtained NiSe/RGO by selenization [32–36]. The oxidation properties of

* Corresponding author. College of Chemistry and Environmental Science, Inner Mongolia Key Laboratory of Green Catalysis and Inner Mongolia Collaborative Innovation Center for Water Environment Safety, Inner Mongolia Normal University, Hohhot, 010022, China.

** Corresponding author.

E-mail addresses: jjc1983@126.com (J. Jia), jml@imnu.edu.cn (M. Jia).

https://doi.org/10.1016/j.ceramint.2019.12.269
Received 4 October 2019; Received in revised form 2 December 2019; Accepted 30 December 2019
Available online 07 January 2020

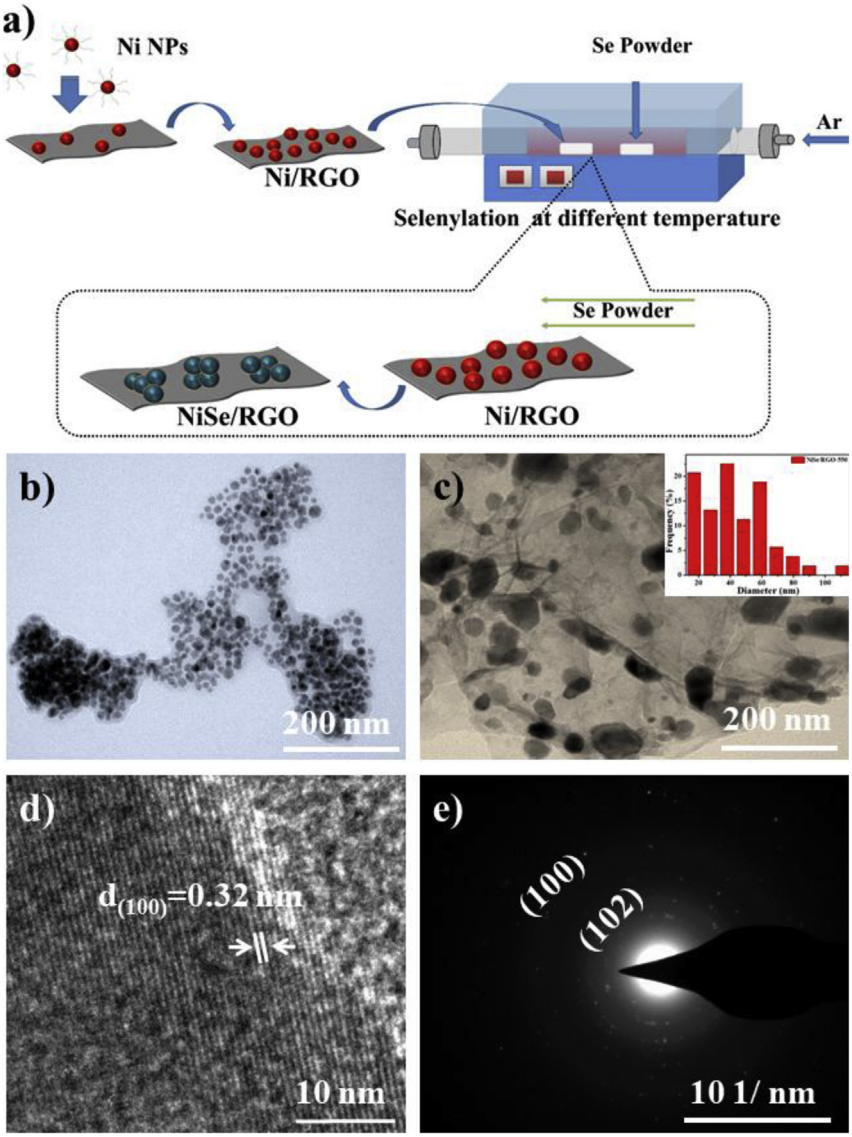

Fig. 1. a) The preparation process for NiSe/RGO. b) TEM images of Ni, c) TEM images of NiSe/RGO-550 d), e) HR-TEM images of NiSe/RGO-550.

methanol were measured in 0.5 M MeOH/1 M KOH solution. NiSe/RGO-550 nanoparticles exhibit excellent methanol oxidation properties. The onset potential of NiSe/RGO-550 nanoparticles (1.35 V *vs.* RHE) is lower than Ni nanoparticles (1.38 V *vs.* RHE), and the peak current density (59.84 mA cm^{-2}) is higher than Ni nanoparticles (13.21 mA cm^{-2}). The NiSe/RGO-550 has a fast kinetic process with a stable catalytic oxidation of methanol more than 4000 s. All experimental results show that NiSe/RGO-550 has superior methanol oxidation performance than Ni nanoparticles.

2. Materials and methods

2.1. Chemicals

Nickel (II) acetylacetonate (98%) and Tri-N-Octylphosphine (TOP, 90%) belong to damas-beta. Hexane, Ethanol and Isopropanol were all AR and received from Sinopharm Group Co. Ltd. Selenium powder (99.9%) and Oleylamine (80–90%) are from Aladdin. Nafion (5 wt%) belongs to the Sigma-Aldrich Chemical Reagent Co. None of the chemicals straightway used in the experiments were further purified.

2.2. Catalysts synthesis

Nickel (II) acetylacetonate (2.0553 g) and TOP (surfactants, 8.8954 g) were dissolved in oleylamine (56 mL) in three flasks. The mixed solution was vigorously stirred for 20 min and heated to 130 °C for 30 min. The compound was further rapidly heated with a step of 5 °C min^{-1} to 200 °C and kept for 30 min. The above steps required the Ar atmosphere protection. The resulting sediment was centrifuged with ethanol, and then the sediment was centrifugal washed with ethanol/isopropanol (Volume ratio = 1:1). Finally, the sediment was dispersed into hexane and naturally dried to obtained Ni nanoparticles.

Ni nanoparticles as-obtained above and reduce graphene oxide (RGO, mass ratio = 100:1) were dissolved in hexane by ultrasound, respectively, then were mixed with a porcelain boat as container, and then selenium powder was put into another porcelain boat on the upstream. The mixture was heated to 550 °C aging about 2 h (at 2 °C min^{-1}) in a tube furnace under an Ar atmosphere. Finally, NiSe/RGO-550 was obtained. In the meantime, we obtained the else calcined specimens under the same conditions except calcination temperature, and the calcination temperature at 450, 650 and 750 °C, respectively. The obtained specimens above were recorded as $NiSe_2$/RGO-450, NiSe/RGO-650 and NiSe/RGO-750, respectively.

2.3. Catalysts characterizations

Powder X-ray diffraction (XRD) were operated to a Rigaku UItima IV. Field emission transmission electron microscopys (FE-TEM) was operated to a Tecnai G2 F20 with voltage of 200 kV and Cu grids was used as substrate. X-ray photoelectron spectroscopy (XPS) was analyzed with an ESCALAB 250Xi.

2.4. Electrochemical measurements

CHI 760E electrochemical workstation (Chenhua Co., Shanghai, China) was operated to electrochemical measurements with three-electrode electrolytic tank at indoor temperature. The counter electrode (Pt net), working electrode (glass carbon electrode, GCE) and reference electrode (Ag/AgCl) were used. The catalyst slurry is composed of Nafion, water and ethanol (volume ratio = 1:9:10). Catalyst (5 mg) was added to catalyst slurry (1 mL), and then the compound was violently ultrasound for 30 min to obtain a uniform compound. A glassy carbon electrode (GCE, 0.07 cm^{-2}) was burnished using alumina powder. Finally, 4 mL of the aforementioned catalyst slurry was uniform drip to the GCE (0.07 cm^{-2}, payload mass of 0.286 mg cm^{-2}) and drying in air at room temperature. All potential values were expressed referenced to the RHE (*vs.* RHE), and all tests have not been iR correction in this work. The cyclic voltammetric (CV) tests and Linear sweep voltammetry (LSV) were performed to research the catalytic competence range 1.1 between 1.7 V *vs.* RHE for MOR. Electrochemical impedance spectroscopy (EIS) of MOR was obtained in the frequency scope between 0.01 Hz and 100 kHz at potential of 1.5 V *vs.* RHE. Chronoamperometry (CA) test was obtained at 1.5 V *vs.* RHE for 4000 s in the same solution. All tests were operated at indoor temperature.

3. Results and discussion

The synthesis process of NiSe/RGO nanoparticles is displayed in Fig. 1a. Nickel (II) acetylacetonate, surfactants (TOP) and solvent (oleylamine) were pyrolyzed to obtained Ni nanoparticles at 200 °C for 30 min. Ni nanoparticles and reduce graphene oxide were mixed evenly and selenylation in tube furnace to obtain NiSe/RGO.

As the TEM diagram of NiSe/RGO-550 shown in Fig. 1c, the NiSe nanoparticles are evenly distributed on the RGO. The illustrations show average particle size of NiSe nanoparticles is 42.8 nm and the lattice spacing is 0.32 nm, corresponding to (100) crystal planes in PDF # 02–0892 (Fig. 1d). Multi-ring bright diffraction ring selected area electron diffraction (SAED) pattern put down to the diffusions from (102), (100) planes of NiSe/RGO-550 (PDF # 02 02–0892), which shows that NiSe/RGO-550 has good crystallinity (Fig. 1e). EDX diagram shows Ni, Se, O, C elements in synthetic compounds, and other impure elements not detected (Fig. S1f). Meanwhile, TEM and HR-TEM images of Ni nanoparticle were shown in Fig. S1. The average particle size of Ni nanoparticle precursor is 11.97 nm (Fig. S1b) and Ni nanoparticles are uniformly distributed with spheres (Figs. 1b and S1a). After selenization, the NiSe/RGO-550 shows anisotropic growth, and the particle size of NiSe/RGO-550 becomes larger [37]. Compared with Fig. S1, Fig. 1 shows that the particle size of nanoparticles increased significantly after selenization. The results showed that NiSe/RGO-550 anisotropic growth increased the particle size and surface area, make the active sites were increased and the catalytic performance may be enhanced [37].

Fig. 2a shows the XRD of NiSe/RGO-550. The sample has incisive diffraction peaks at 27.857°, 32.778°, 44.369°, 49,931°, 59.555°, 61.164°, 69.055°, 70.417°, which can be corresponds to (100), (101), (102), (110), (103), (201), (202), (004) crystallographic plane of hexagonal NiSe (ICDD PDF card 02–0892), respectively. No diffraction peaks of other impurities are observed, indicating that NiSe was successfully prepared. The XRD pattern of the precursor Ni was shown in Fig. S2a. Compared with Fig. S2a, Fig. 2a shows no peak of pure Ni after selenization, indicating that selenization was more thorough. In addition, in order to compare the MOR performance of NiSe/RGO-550, we also obtained nickel selenide at different temperatures, as shown in Fig. S2b. $NiSe_2$ was prepared at 450 °C (denote as $NiSe_2$/RGO-450), NiSe also were prepared at 650 and 750 °C (denote as NiSe/RGO-650 and NiSe/RGO-750). As selenation temperature from 450 °C to 550 °C, the content of selenium decreases because of the evaporation of selenium power. While increasing from 550 °C to 750 °C, 550 °C becomes the best calcined temperature may be due to the influence of thermal stability of selenide [38].

The XPS diagram shows the chemical composition of NiSe/RGO-550, and the full spectrum shows the C, O, Ni, Se elements (Fig. S3). The C=C, C–C (sp^3), C–O of C 1s at 283.7, 285.0 and 285.9 eV [21,39], respectively (Fig. 2b). The peak of Ni $2p_{3/2}$ and Ni $2p_{1/2}$ at 854.6 and 872.0 eV, and shakeup satellites at 860.1 and 878.6 eV, respectively, indicated that Ni exists in the form of Ni^{2+} in NiSe [18,22,40] (Fig. 2c). The binding energies at 851.7 and 869.1 eV were corresponding to metallic Ni of Ni $2p_{3/2}$ and Ni $2p_{1/2}$ [41,42]. The peak of 53.6, 55.7 and 57.8 eV was assigned to Se $3d_{5/2}$, Se $3d_{3/2}$ and SeO_x (oxidation state of Se) [18,25,42–45] (Fig. 2d). The XPS results showed that the NiSe/RGO-550 catalyst was prepared successfully.

Fig. 3a and b and Figs. S4a, c, e shows the CV of Ni, NiSe/RGO-550, $NiSe_2$/RGO-450, NiSe/RGO-650 and NiSe/RGO-750 in 1 M KOH at disparate sweep speeds, respectively. The peak current density augment with the sweep rates, the anode peak current moves forward to the high potential, while the cathode peak current density shifts forward to the low potential. The peak current density is related to the limitation of reaction kinetics. We hypothesized that the redox peak was with the mutual transformation of $Ni(OH)_2$ and NiOOH, that is to say the mutual transformation of Ni^{2+} and Ni^{3+} for MOR [32].

The peak ampere density (I_p) in direct proportion to the square root of the scan rate ($\nu^{1/2}$) in 5–60 mV s^{-1}, as the Ip *vs.* $\nu^{1/2}$ (Fig. 3c, d and Figs. S4b, d, f), indicated the diffusion-limited redox reaction [30,32,46,47].

$$I_p = 2.69 \times 10^5 n^{3/2} A D^{1/2} C \nu^{1/2}$$

In the above formula, n represents the amount of metastasizing electrons, D represents the diffusion coefficient of the reactant, A represents the geometric acreage of the working electrode and C represents the initial concentration of the reduzate. I_p has a positive correlation with $\nu^{1/2}$, and $Ni(OH)_2 \leftrightarrow NiOOH$ oxidation process is usually deemed to be a rate-determining step of the proton diffusion. Therefore, according to the above formula, proton diffusion coefficient of NiSe/RGO-550 is 2.36 × 10^{-6} cm^2 s^{-1}, and proton diffusion coefficient of Ni is 7.85 × 10^{-8} cm^2 s^{-1}. Because of the augment of active sites after selenization and the load of RGO enhanced electroconductibility, the diffusion coefficient increases which are more conducive to the diffusion of active species [5,48,49].

The CV bights of different methanol concentrations in 1 M KOH were recorded in Fig. S5. When the methanol concentration is lower than 0.5 M, the catalytic performance of NiSe/RGO-550 is poor may be due to the low methanol concentration. When the concentration of methanol is too high, methanol molecules could cover NiSe/RGO-550, making its MOR performance poor [29,50,51]. Therefore, the MOR performance all samples were tested in 0.5 M MeOH/1 M KOH. Fig. 4a and b demonstrates the CVs of Ni and NiSe/RGO-550 in the presence and absence of 0.5 M methanol, we observed that the peak anodic oxidation current of NiSe/RGO-550 and Ni increased significantly in the presence of 0.5 M methanol, indicating that both NiSe/RGO-550 and Ni had MOR properties. The peak current density of NiSe/RGO-550 (59.84 mA cm^{-2}) is higher than Ni (13.21 mA cm^{-2}), which may due to NiSe loaded on RGO to improve the synergy between NiSe and RGO, and the conductivity of RGO improves the conductivity of catalysts. The methanol oxidation reaction mechanism of NiSe/RGO-550 may be further explained by equations (1) and (2). Methanol oxidation reaction

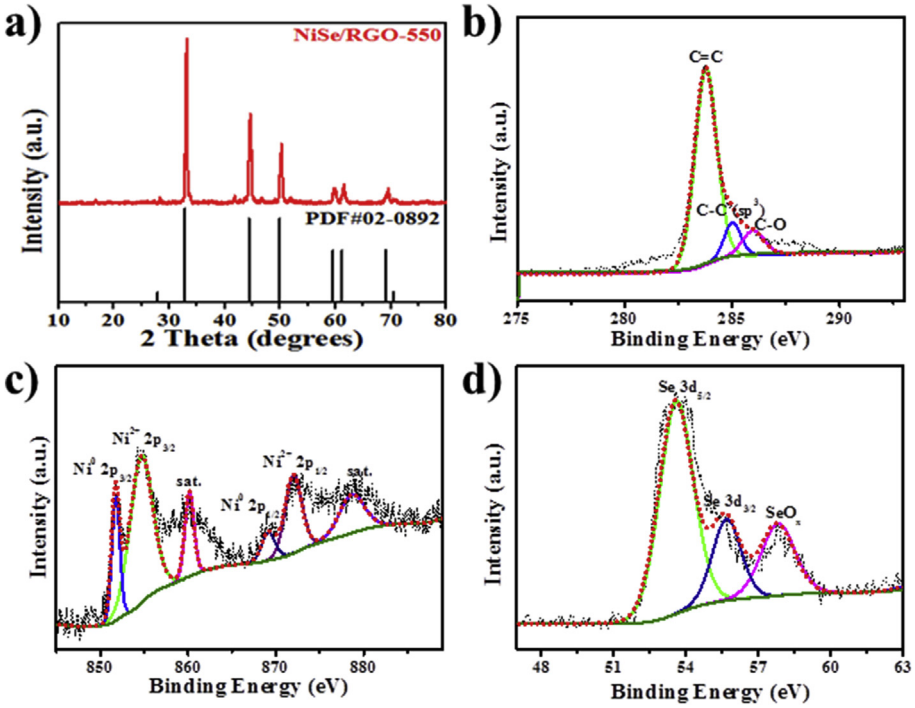

Fig. 2. a) XRD of NiSe/RGO-550, the corresponding high-resolution XPS spectrums of b) C1s, c) Ni 2p and d) Se 3d.

may occur in the following two processes. First, Ni^{2+} in NiSe/RGO-550 is oxidized to a high valence state of Ni^{3+}. In the second stage, the high valence states Ni^{3+} was reduced to the low valence states Ni^{2+} in the methanol oxidation process [1,30]. In addition, the methanol oxidation activity of NiSe/RGO-550 is also higher than $NiSe_2$/RGO-450 (44.20 mA cm^{-2}), NiSe/RGO-650 (46.50 mA cm^{-2}) and NiSe/RGO-750 (29.53 mA cm^{-2}) in Fig. 5a. The onset potential of NiSe/RGO-550 is 1.35 V *vs.* RHE lower than Ni (1.38 V *vs.* RHE), which is displayed in the LSV curves (Fig. 5b). It shows that NiSe/RGO-550 has a fast kinetic process for methanol oxidation.

$$Ni(OH)_2 + OH^- \rightarrow NiOOH + H_2O + e^- \quad (1)$$

$$NiOOH + CH_3OH + 1.25O_2 \rightarrow Ni(OH)_2 + CO_2 + 1.5H_2O \quad (2)$$

The electrochemical impedance spectroscopy (EIS) of NiSe/RGO and Ni was tested at 1.5 V *vs.* RHE for MOR. Fig. 5c shows the EIS diagrams of NiSe/RGO-550, Ni and nickel selenide obtained at different temperatures. The spectra are all single semicircle. It shows that the

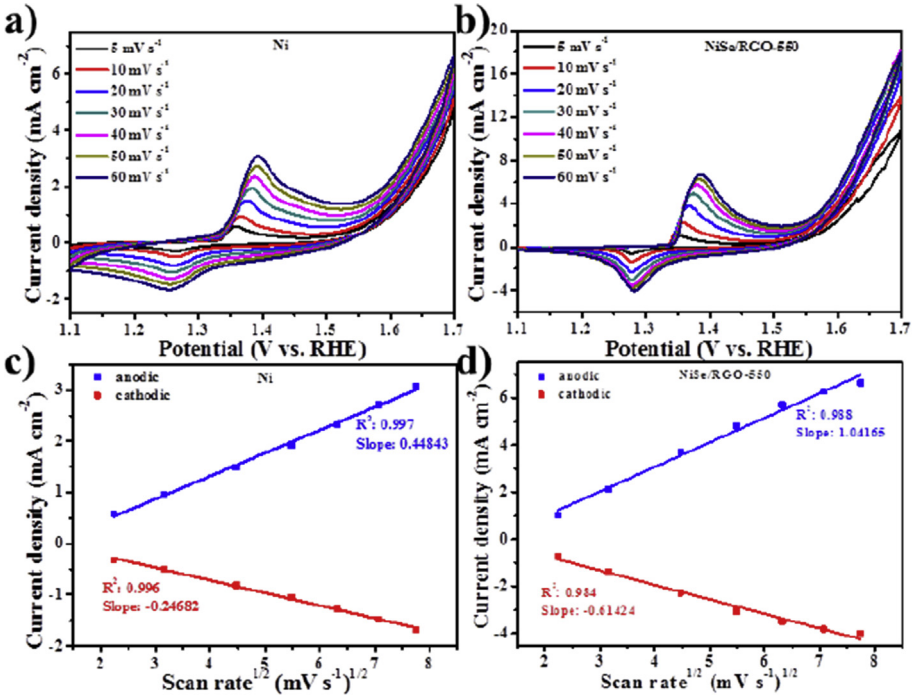

Fig. 3. a) CV of Ni and b) NiSe/RGO-550 in 1 M KOH from 5 to 60 mV s^{-1}. c), d) linear relation of the anodal and cathodal peak current density versus the square roots of the sweep speed in the sweep speed scope (5–60 mV s^{-1}) for Ni and NiSe/RGO-550.

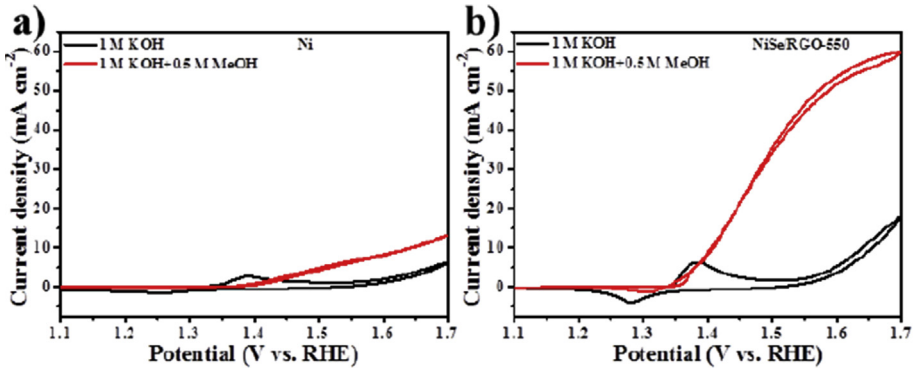

Fig. 4. a) Ni and b) NiSe/RGO-550 in 1 M KOH solution existence and nonexistence 0.5 M MeOH with a sweep speed of 50 mV s^{-1}.

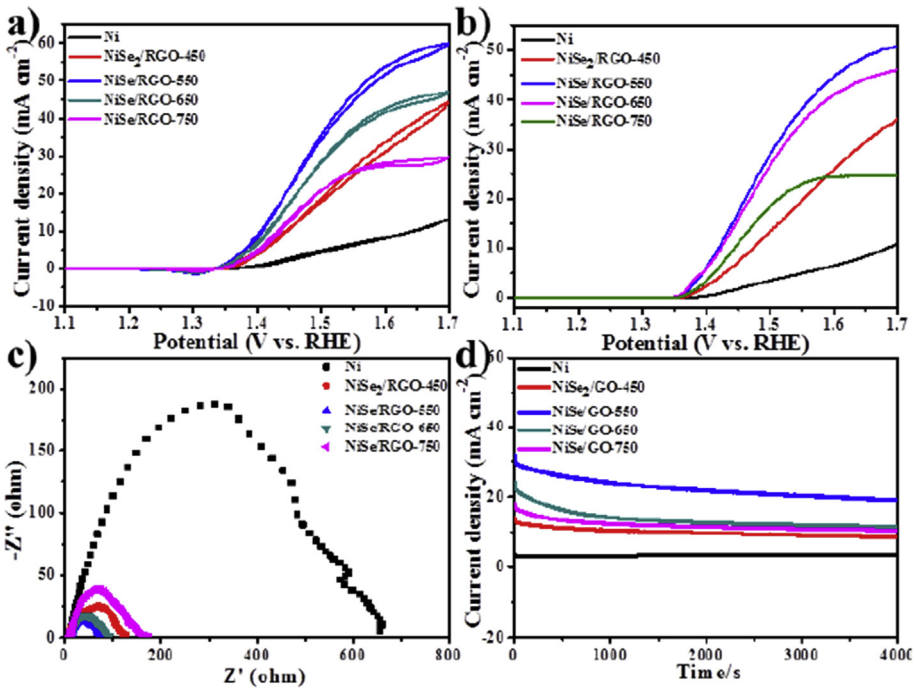

Fig. 5. a) Comparison CV bights of Ni, NiSe$_2$/RGO-450, NiSe/RGO-550, NiSe/RGO-650 and NiSe/RGO-750 in 0.5 M MeOH/1 M KOH with a sweep speed of 50 mV s^{-1}; b) Comparison LSVs of Ni, NiSe$_2$/RGO-450, NiSe/RGO-550, NiSe/RGO-650 and NiSe/RGO-750 in 0.5 M MeOH/1 M KOH with a sweep speed of 5 mV s^{-1}; c) EIS curves of Ni, NiSe$_2$/RGO-450, NiSe/RGO-550, NiSe/RGO-650 and NiSe/RGO-750 in 0.5 M MeOH/1 M KOH with potential of 1.5 V *vs.* RHE; d) Comparison Chronoamperometry curves of Ni, NiSe$_2$/RGO-450, NiSe/RGO-550, NiSe/RGO-650 and NiSe/RGO-750 in 0.5 M MeOH/1 M KOH solution with potential of 1.5 V *vs.* RHE.

NiSe/RGO-550 has the smallest semicircle radius, while Ni has the largest semicircle radius. The decrease of semicircle radius means the reducing of charge transfer resistance (R_{ct}) of MOR, this may be related to RGO as a supporter to enhance the electrical conductivity of nickel selenide, and speed the charge transfer.

The stability of NiSe/RGO-550 and Ni was tested for 4000s by Chronoamperometry with the potential of 1.5 V *vs.* RHE. At the beginning of chronoamperometry, the NiSe/RGO-550 have a current density declined slightly, which is possibly due to the active site of catalyst did not adsorb methanol molecules. It may also be on account of the formation of intermediates of the reaction at the initial stage, which makes the catalyst poisoning and the current density decreases. When the new methanol molecules were adsorbed at the active site, it made the catalytic activity tend to be stable [29]. The current density of NiSe/RGO-550 is higher than Ni and nickel selenide obtained at different temperatures (Fig. 5d), manifesting that the NiSe/RGO-550 has better stability of methanol oxidation.

The excellent MOR performance of NiSe/RGO-550 is memorably. The NiSe/RGO-550 has outstanding MOR performance. The low onset potential, supernal peak current density, and the synthetic NiSe/RGO-550 are outstanding compared to Ni, which may be impute the following factors. (1) Nanoparticles architecture offer rich active reaction sites. (2) The increase of active sites after selenization. (3) The load of RGO enhanced electrical conductivity, which is more conducive to the diffusion of active species.

4. Conclusions

In summary, we have resoundingly prepared NiSe/RGO-550 nanoparticles by a simple and universal way that pyrolyzation and selenylation. The electrochemical catalytic activity of methanol oxidation of NiSe/RGO-550 nanoparticles was measured, and the consequences showed that the NiSe/RGO-550 nanoparticles has a supernal electrochemical catalytic competence of methanol oxidation than Ni and other nickel selenide obtained at disparate temperatures. Hence, the outstanding methanol oxidation performance of NiSe/RGO-550 nanoparticles indicates that NiSe/RGO-550 nanoparticle is a promising anode material for DMFCs. This work provides the possibility for the preparation and application of other nickel-based non-noble metal catalysts.

Declaration of competing interest

The authors declare that they have no known competing financial interests or personal relationships that could have appeared to influence the work reported in this paper.

Acknowledgements

We would like to thank National Natural Science Foundation of China (Project No.21703249), the Research Foundation for Advanced Talents of Inner Mongolia Normal University (No.2018YJRC001, 2018YJRC012), and the Foundation of Fujian Provincial Key Laboratory of Fire Retardant Materials (FH201802) for financial support.

Appendix A. Supplementary data

Supplementary data to this article can be found online at https://doi.org/10.1016/j.ceramint.2019.12.269.

References

[1] B. Dong, W. Li, X. Huang, Z. Ali, T. Zhang, Z. Yang, Y. Hou, Fabrication of hierarchical hollow Mn doped $Ni(OH)_2$ nanostructures with enhanced catalytic activity towards electrochemical oxidation of methanol, Nano Energy 55 (2019) 37–41.
[2] G. Arteaga, L.M. Rivera-Gavidia, S.J. Martínez, R. Rizo, E. Pastor, G. García, Methanol oxidation on graphenic-supported platinum catalysts, Surfaces 2 (2019) 16–31.
[3] U. Burke, W.K. Metcalfe, S.M. Burke, K.A. Heufer, P. Dagaut, H.J. Curran, A detailed chemical kinetic modeling, ignition delay time and jet-stirred reactor study of methanol oxidation, Combust. Flame 165 (2016) 125–136.
[4] O. Akyıldırım, H. Yüksek, H. Saral, İ. Ermiş, T. Eren, M.L. Yola, Platinum nanoparticles supported on nitrogen and sulfur-doped reduced graphene oxide nanomaterial as highly active electrocatalysts for methanol oxidation, J. Mater. Sci. Mater. Electron. 27 (2016) 8559–8566.
[5] L. Dong, R.R.S. Gari, Z. Li, M.M. Craig, S. Hou, Graphene-supported platinum and platinum–ruthenium nanoparticles with high electrocatalytic activity for methanol and ethanol oxidation, Carbon 48 (2010) 781–787.
[6] X. Du, S. Luo, H. Du, M. Tang, X. Huang, P.K. Shen, Monodisperse and self-assembled Pt-Cu nanoparticles as an efficient electrocatalyst for the methanol oxidation reaction, J. Mater. Chem. 4 (2016) 1579–1585.
[7] D.H. Kim, D.-Y. Shin, Y.-G. Lee, G.-H. An, J.H. Han, H.-J. Ahn, B.J. Choi, Effects of SnO_2 layer coated on carbon nanofiber for the methanol oxidation reaction, Ceram. Int. 44 (2018) 19554–19559.
[8] G.F. Long, X.H. Li, K. Wan, Z.X. Liang, J.H. Piao, P. Tsiakaras, Pt/CN-doped electrocatalysts: superior electrocatalytic activity for methanol oxidation reaction and mechanistic insight into interfacial enhancement, Appl. Catal. B Environ. 203 (2017) 541–548.
[9] J.H. Ma, L. Wang, X. Mu, L. Li, Nitrogen-doped graphene supported Pt nanoparticles with enhanced performance for methanol oxidation, Int. J. Hydrogen Energy 40 (2015) 2641–2647.
[10] Y. Qin, L. Chao, J. Yuan, Y. Liu, F. Chu, Y. Kong, Y. Tao, M. Liu, Ultrafine Pt nanoparticle-decorated robust 3D N-doped porous graphene as an enhanced electrocatalyst for methanol oxidation, Chem. Commun. 52 (2016) 382–385.
[11] X. Zhao, L. Dai, Q. Qin, F. Pei, C. Hu, N. Zheng, Self-Supported 3D PdCu alloy nanosheets as a bifunctional catalyst for electrochemical reforming of ethanol, Small 13 (2017) 1602970.
[12] L. Huang, X. Luo, Y. Jiang, X. Mao, M. Shi, Oxygen deficiency assisted synthesis of network-like tungsten carbide-carbon nanotubes composites for methanol oxidation, Ceram. Int. 45 (2019) 16976–16981.
[13] S. Eris, Z. Daşdelen, Y. Yıldız, F. Sen, Nanostructured Polyaniline-rGO decorated platinum catalyst with enhanced activity and durability for Methanol oxidation, Int. J. Hydrogen Energy 43 (2018) 1337–1343.
[14] Y. Yıldız, S. Kuzu, B. Sen, A. Savk, S. Akocak, F. Şen, Different ligand based monodispersed Pt nanoparticles decorated with rGO as highly active and reusable catalysts for the methanol oxidation, Int. J. Hydrogen Energy 42 (2017) 13061–13069.
[15] Z. Ozturk, F. Sen, S. Sen, G. Gokagac, The preparation and characterization of nano-sized Pt–Pd/C catalysts and comparison of their superior catalytic activities for methanol and ethanol oxidation, J. Mater. Sci. 47 (2012) 8134–8144.
[16] E. Erken, Y. Yıldız, B. Kilbaş, F. Şen, Synthesis and characterization of nearly monodisperse Pt nanoparticles for C1 to C3 alcohol oxidation and dehydrogenation of dimethylamine-borane (DMAB), J. Nanosci. Nanotechnol., 16 (6), 5944-5950..
[17] Y. Wang, J. Wang, G. Han, C. Du, Q. Deng, Y. Gao, G. Yin, Y. Song, Pt decorated Ti_3C_2 MXene for enhanced methanol oxidation reaction, Ceram. Int. 45 (2019) 2411–2417.
[18] Y. Du, G. Cheng, W. Luo, Colloidal synthesis of urchin-like Fe doped $NiSe_2$ for efficient oxygen evolution, Nanoscale 9 (2017) 6821–6825.
[19] R. Gao, G.D. Li, J. Hu, Y. Wu, X. Lian, D. Wang, X. Zou, In situ electrochemical formation of NiSe/NiOx core/shell nano-electrocatalysts for superior oxygen evolution activity, Catalysis Science & Technology 6 (2016) 8268–8275.
[20] Z. Gao, J. Qi, M. Chen, W. Zhang, R. Cao, An electrodeposited NiSe for electrocatalytic hydrogen and oxygen evolution reactions in alkaline solution, Electrochim. Acta 224 (2017) 412–418.
[21] X. Han, X. Tong, G. Wu, N. Yang, X.-Y. Guo, Carbon fibers supported NiSe nanowire arrays as efficient and flexible electrocatalysts for the oxygen evolution reaction, Carbon 129 (2018) 245–251.
[22] Y. Li, D. Yan, Y. Zou, C. Xie, Y. Wang, Y. Zhang, S. Wang, Rapidly engineering the electronic properties and morphological structure of NiSe nanowires for the oxygen evolution reaction, J. Mater. Chem. 5 (2017) 25494–25500.
[23] M.R. Gao, Z.Y. Lin, T.T. Zhuang, J. Jiang, Y.F. Xu, Y.R. Zheng, S.H. Yu, Mixed-solution synthesis of sea urchin-like NiSe nanofiber assemblies as economical Pt-free catalysts for electrochemical H_2 production, J. Mater. Chem. 22 (2012) 13662.
[24] Y. Huang, X. Chong, C. Liu, Y. Liang, B. Zhang, Boosting hydrogen production by anodic oxidation of primary amines over a NiSe nanorod electrode, Angew. Chem. Int. Ed. 57 (2018) 13163–13166.
[25] Q. Luo, M. Peng, X. Sun, A.M. Asiri, In situ growth of nickel selenide nanowire arrays on nickel foil for methanol electro-oxidation in alkaline media, RSC Adv. 5 (2015) 87051–87054.
[26] Z. Zhang, L. Xin, K. Sun, W. Li, Pd–Ni electrocatalysts for efficient ethanol oxidation reaction in alkaline electrolyte, Int. J. Hydrogen Energy 36 (2011) 12686–12697.
[27] M.A. Abdel Rahim, R.M. Abdel Hameed, M.W. Khalil, Nickel as a catalyst for the electro-oxidation of methanol in alkaline medium, J. Power Sources 134 (2004) 160–169.
[28] L.L. Carvalho, F. Colmati, A.A. Tanaka, Nickel–palladium electrocatalysts for methanol, ethanol, and glycerol oxidation reactions, Int. J. Hydrogen Energy 42 (2017) 16118–16126.
[29] X. Cui, W. Guo, M. Zhou, Y. Yang, Y. Li, P. Xiao, Y. Zhang, X. Zhang, Promoting effect of Co in Ni_mCo_n (m + n = 4) bimetallic electrocatalysts for methanol oxidation reaction, ACS Appl. Mater. Interfaces 7 (2015) 493–503.
[30] E. Umeshbabu, G. Ranga Rao, $NiCo_2O_4$ hexagonal nanoplates anchored on reduced graphene oxide sheets with enhanced electrocatalytic activity and stability for methanol and water oxidation, Electrochim. Acta 213 (2016) 717–729.
[31] W. Wang, Q. Chu, Y. Zhang, W. Zhu, X. Wang, X. Liu, Nickel foam supported mesoporous $NiCo_2O_4$ arrays with excellent methanol electro-oxidation performance, New J. Chem. 39 (2015) 6491–6497.
[32] J. Li, Z. Luo, F. He, Y. Zuo, C. Zhang, J. Liu, X. Yu, R. Du, T. Zhang, M.F. Infante-Carrió, P. Tang, J. Arbiol, J. Llorca, A. Cabot, Colloidal Ni–Co–Sn nanoparticles as efficient electrocatalysts for the methanol oxidation reaction, J. Mater. Chem. 6 (2018) 22915–22924.
[33] V. Mazumder, M. Chi, M.N. Mankin, Y. Liu, O. Metin, D. Sun, K.L. More, S. Sun, A facile synthesis of MPd (M = Co, Cu) nanoparticles and their catalysis for formic acid oxidation, Nano Lett. 12 (2012) 1102–1106.
[34] X. Fan, Z. Peng, R. Ye, H. Zhou, X. Guo, M_3C (M: Fe, Co, Ni) nanocrystals encased in graphene nanoribbons: an active and stable bifunctional electrocatalyst for oxygen reduction and hydrogen evolution reactions, ACS Nano 9 (2015) 7407–7418.
[35] C.M. Hessel, V.P. Pattani, M. Rasch, M.G. Panthani, B. Koo, J.W. Tunnell, B.A. Korgel, Copper selenide nanocrystals for photothermal therapy, Nano Lett. 11 (2011) 2560–2566.
[36] Ö. Metin, S.F. Ho, C. Alp, H. Can, M.N. Mankin, M.S. Gültekin, M. Chi, S. Sun, Ni/Pd core/shell nanoparticles supported on graphene as a highly active and reusable catalyst for Suzuki-Miyaura cross-coupling reaction, Nano Research 6 (2013) 10–18.
[37] A. Mendoza-Garcia, H. Zhu, Y. Yu, Q. Li, L. Zhou, D. Su, M.J. Kramer, S. Sun, Controlled anisotropic growth of Co-Fe-P from Co-Fe-O nanoparticles, Angew. Chem. Int. Ed. 127 (2015) 9778–9781.
[38] C. Guillén, J. Herrero, Nanocrystalline copper sulfide and copper selenide thin films with p-type metallic behavior, J. Mater. Sci. 52 (2017) 13886–13896.
[39] J.K. Kim, G.D. Park, J.H. Kim, S.K. Park, Y.C. Kang, Rational design and synthesis of extremely efficient macroporous CoSe2 -CNT composite microspheres for hydrogen evolution reaction, Small 13 (2017) 1700068.
[40] K. Guo, F. Yang, S. Cui, W. Chen, L. Mi, Controlled synthesis of 3D hierarchical NiSe microspheres for high-performance supercapacitor design, RSC Adv. 6 (2016) 46523–46530.
[41] C. Tang, Z. Pu, Q. Liu, A.M. Asiri, X. Sun, Y. Luo, Y. He, In Situ growth of NiSe nanowire film on nickel foam as an electrode for high-performance supercapacitors, ChemElectroChem 2 (2015) 1903–1907.
[42] X. Li, G.Q. Han, Y.R. Liu, B. Dong, W.H. Hu, X. Shang, Y.M. Chai, C.G. Liu, NiSe@NiOOH core-shell hyacinth-like nanostructures on nickel foam synthesized by in situ electrochemical oxidation as an efficient electrocatalyst for the oxygen evolution reaction, ACS Appl. Mater. Interfaces 8 (2016) 20057–20066.
[43] C. Bao, F. Li, J. Wang, P. Sun, N. Huang, Y. Sun, L. Fang, L. Wang, X. Sun, One-pot solvothermal in situ growth of 1D single-crystalline NiSe on Ni foil as efficient and stable transparent conductive oxide free counter electrodes for dye-sensitized solar cells, ACS Appl. Mater. Interfaces 8 (2016) 32788–32796.
[44] U. Subbarao, V.S. Marakatti, M.K. Amshumali, B. Loukya, D.K. Singh, R. Datta, S.C. Peter, Size and morphology controlled NiSe nanoparticles as efficient catalyst for the reduction reactions, J. Solid State Chem. 244 (2016) 84–92.
[45] Z.Z. Tian Yanping, Miao Yuqing, Co-Te-Se nano-compounds as electrocatalysts for hydrogen evolution reaction, J. Electrochem. Soc. 163 (2016) H625–H629.
[46] X. Guo, T. Liang, D. Zhang, M. Zhang, Y. Lin, C. Lai, Facile fabrication of 3D porous nickel networks for electro-oxidation of methanol and ethanol in alkaline medium, Mater. Chem. Phys. 221 (2019) 390–396.
[47] J. Li, Z. Luo, Y. Zuo, J. Liu, T. Zhang, P. Tang, J. Arbiol, J. Llorca, A. Cabot, NiSn bimetallic nanoparticles as stable electrocatalysts for methanol oxidation reaction, Appl. Catal. B Environ. 234 (2018) 10–18.
[48] X. Zhang, M. Zhen, J. Bai, S. Jin, L. Liu, Efficient NiSe-Ni_3Se_2/graphene electrocatalyst in dye-sensitized solar cells: the role of hollow hybrid nanostructure, ACS Appl. Mater. Interfaces 8 (2016) 17187–17193.
[49] X. Zhang, T.Z. Jing, S.Q. Guo, G.D. Gao, L. Liu, Synthesis of $NiSe_2$/reduced graphene oxide crystalline materials and their efficient electrocatalytic activity in dye-sensitized solar cells, RSC Adv. 4 (2014) 50312–50317.
[50] I.S. Pieta, A. Rathi, P. Pieta, R. Nowakowski, M. Hołdynski, M. Pisarek, A. Kaminska, M.B. Gawande, R. Zboril, Electrocatalytic methanol oxidation over Cu, Ni and bimetallic Cu-Ni nanoparticles supported on graphitic carbon nitride, Appl. Catal. B Environ. 244 (2019) 272–283.
[51] S. Rezaee, S. Shahrokhian, Facile synthesis of petal-like NiCo/NiO-CoO/nanoporous carbon composite based on mixed-metallic MOFs and their application for electrocatalytic oxidation of methanol, Appl. Catal. B Environ. 244 (2019) 802–813.